

Neutron skin of ^{48}Ca consistent with experimental data on skins

Shingo Tagami,¹ Jun Matsui,¹ Maya Takechi,² and Masanobu Yahiro^{1,*}

¹*Department of Physics, Kyushu University, Fukuoka 812-8581, Japan*

²*Niigata University, Niigata 950-2181, Japan*

Background: In our previous paper, we predicted neutron skin r_{skin} and proton, neutron, matter radii, r_p , r_n , r_m for $^{40-60,62,64}\text{Ca}$ after determining the neutron dripline, using the Gogny-D1S Hartree-Fock-Bogoliubov (GHFB) with and without the angular momentum projection (AMP). We found that effects of the AMP are small. Very lately, Tanaka *et al.* measured interaction cross sections σ_I for $^{42-51}\text{Ca}$, determined matter radii $r_m(\sigma_I)$ from the σ_I , and deduced skin $r_{\text{skin}}(\sigma_I)$ and $r_n(\sigma_I)$ from the $r_m(\sigma_I)$ and the $r_p(\text{exp})$ evaluated from the electron scattering. Comparing our results with the data, we find for $^{42-48}\text{Ca}$ that GHFB and GHFB+AMP reproduce $r_{\text{skin}}(\sigma_I)$, $r_n(\sigma_I)$, $r_m(\sigma_I)$, but not for $r_p(\text{exp})$.

Aim: Our purpose is to determine a value of r_{skin}^{48} by using GHFB+AMP and the constrained GHFB (cGHFB) in which the calculated value is fitted to $r_p(\text{exp})$.

Results: For $^{42,44,46,48}\text{Ca}$, cGHFB hardly changes r_{skin} , r_m , r_n calculated with GHFB+AMP, except for r_{skin}^{48} . For r_{skin}^{48} , the cGHFB result is $r_{\text{skin}}^{48} = 0.190$ fm, while $r_{\text{skin}}^{48} = 0.159$ fm for GHFB+AMP. We should take the upper and the lower bound of GHFB+AMP and cGHFB. The result $r_{\text{skin}}^{48} = 0.159 - 0.190$ fm consists with the $r_{\text{skin}}^{48}(\sigma_I)$ and the data $r_{\text{skin}}^{48}(E1pE)$ obtained from high-resolution $E1$ polarizability experiment ($E1pE$). Using the $r_{\text{skin}}^{48} - r_{\text{skin}}^{208}$ relation with strong correlation of Ref. [3], we transform the data r_{skin}^{208} determined by PREX and $E1pE$ to the corresponding values, $r_{\text{skin}}^{48}(\text{tPREX})$ and $r_{\text{skin}}^{48}(\text{tE1pE})$, where the symbol ‘t’ stands for the transformed data. Our result is consistent also for $r_{\text{skin}}^{48}(\text{tPREX})$ and $r_{\text{skin}}^{48}(\text{tE1pE})$. Eventually, for $^{42,44,46,48}\text{Ca}$, cGHFB reproduces $r_{\text{skin}}(\sigma_I)$, $r_m(\sigma_I)$, $r_n(\sigma_I)$, $r_p(\text{exp})$, while GHFB+AMP does $r_{\text{skin}}(\sigma_I)$, $r_m(\sigma_I)$, $r_n(\sigma_I)$.

I. INTRODUCTION AND CONCLUSION

Background on experiments. Neutron skin thickness r_{skin} is strongly correlated with the sloop parameter L in the symmetric energy of nuclear matter [1–3]. The r_{skin} is thus important to determine the EoS.

Horowitz, Pollock and Souder proposed a direct measurement for $r_{\text{skin}} = r_n - r_p$ [4], where r_p and r_n are proton and neutron radii, respectively. The measurement consists of parity-violating and elastic electron scattering. The r_n is determined from the former experiment, and the r_p is from the latter. For r_{skin}^{208} , in fact, the Lead Radius EXperiment (PREX) [5–7] yields

$$r_{\text{skin}}^{208}(\text{PREX}) = 0.33_{-0.18}^{+0.16} = 0.15 - 0.49 \text{ fm.} \quad (1)$$

The result has a large error. For this reason, the PREX-II and the ^{48}Ca Radius EXperiment (CREX) are ongoing at Jefferson Lab [5].

As an indirect measurement on r_{skin} , the high-resolution $E1$ polarizability experiment ($E1pE$) was made for ^{208}Pb [8] and ^{48}Ca [9] in RCNP. The results are

$$r_{\text{skin}}^{208}(E1pE) = 0.156_{-0.021}^{+0.025} = 0.135 - 0.181 \text{ fm,} \quad (2)$$

$$r_{\text{skin}}^{48}(E1pE) = 0.14 - 0.20 \text{ fm.} \quad (3)$$

For ^{208}Pb , the central value 0.156 fm of the indirect measurement is much smaller than 0.33 fm of the direct measurement. This is a problem to be solved.

Very lately, Tanaka *et al.* published data on interaction cross sections σ_I for $^{42-51}\text{Ca}$ [10]. The data have high accuracy, since the average error is 1.05%. They determined

$r_m(\sigma_I)$ from the σ_I using the Glauber model, and deduced $r_{\text{skin}}(\sigma_I)$ and $r_n(\sigma_I)$ from the $r_m(\sigma_I)$ and the $r_p(\text{exp})$ of Ref. [11]. For ^{48}Ca , a value of $r_{\text{skin}}(\sigma_I)$ is

$$r_{\text{skin}}^{48}(\sigma_I) = 0.086 - 0.206 \text{ fm.} \quad (4)$$

Using the $r_{\text{skin}}^{48} - r_{\text{skin}}^{208}$ relation [3] with high correlation coefficient of $R = 0.99$,

$$r_{\text{skin}}^{48} = 0.5547 r_{\text{skin}}^{208} + 0.0718, \quad (5)$$

we transform $r_{\text{skin}}^{208}(\text{PREX})$ and $r_{\text{skin}}^{208}(E1pE)$ to the corresponding values $r_{\text{skin}}^{48}(\text{tPREX})$ and $r_{\text{skin}}^{48}(\text{tE1pE})$, where the symbol ‘t’ stands for the transformed data. The transformed data are

$$r_{\text{skin}}^{48}(\text{tPREX}) = 0.155 - 0.344 \text{ fm} \quad (6)$$

for PREX and

$$r_{\text{skin}}^{48}(\text{tE1pE}) = 0.147 - 0.172 \text{ fm} \quad (7)$$

for $E1pE$.

Background on theories: As an *ab initio* method for Ca isotopes, we should consider the coupled-cluster method [12, 13] with chiral interaction. The coupled-cluster result [12]

$$r_{\text{skin}}^{48}(\text{CC}) = 0.12 - 0.15 \text{ fm} \quad (8)$$

is consistent with data $r_{\text{skin}}^{48}(E1pE)$ and $r_{\text{skin}}^{48}(\sigma_I)$.

Among effective interactions, NNLO_{sat} [14] is a chiral interaction constrained by radii and binding energies of selected nuclei up to $A \approx 25$ [12], where A is the mass number. In fact, the *ab initio* calculations were done for Ca isotopes [12, 14, 15]. As shown in Fig. 1, Garcia Ruiz *et al.* evaluated the charge radii R_{ch} for $^{39-54}\text{Ca}$ [15], using the coupled-cluster method with two low-momentum effective interactions, SRG1 of Ref. [16] and SRG2 of Ref. [17], that are derived from the chiral interaction with the renormalization

* orion093g@gmail.com

group method. The SRG1 (SRG2) yields the lower (upper) bound of r_{ch} . Difference of the two results is ~ 1.2 fm.

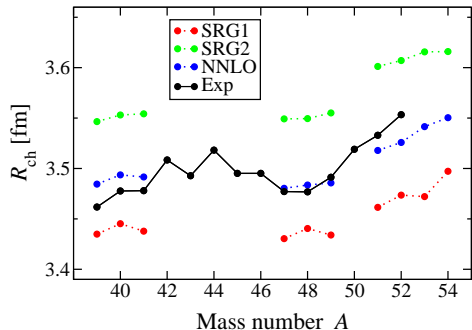


FIG. 1. A dependence of charge radii R_{ch} for $^{40-54}\text{Ca}$ taken from Ref. [15].

In our previous paper of Ref. [18], we predicted r_p , r_n , matter radii r_m , r_{skin} for $^{40-60,62,64}\text{Ca}$ after determining the neutron dripline, using the Gogny-D1S Hartree-Fock-Bogoliubov (GHFB) with the angular momentum projection (AMP) [19] for even nuclei and GHFB for odd nuclei. For odd nuclei, GHFB+AMP calculations are not feasible. The reason is shown in Sec. II A. Using the Kyushu (chiral) g -matrix folding model [20–22], we also predicted reaction cross section σ_R for $^{40-60,62,64}\text{Ca}$ scattering on a ^{12}C target at 280 MeV/nucleon, since Tanaka *et al.* measured interaction cross sections $\sigma_I (\approx \sigma_R)$ for $^{42-51}\text{Ca}$.

In our previous paper, we first confirmed that effects of the AMP are small for even nuclei. GHFB and GHFB+AMP reproduce the one-neutron separation energy S_1 and the two-neutron separation energy S_2 in $^{41-58}\text{Ca}$ [23–25]. Using S_1 and S_2 , we found that ^{64}Ca is an even-dripline nucleus and ^{59}Ca is an odd-dripline nucleus. As for E_B , our results are consistent with the data [23] in $^{40-58}\text{Ca}$. Comparing our results with new data of Ref. [10], we find for $^{42-48}\text{Ca}$ that GHFB and GHFB+AMP reproduce $r_{\text{skin}}(\sigma_I)$, $r_n(\sigma_I)$, $r_m(\sigma_I)$, but not for $r_p(\text{exp})$.

Aim and conclusion: In this paper, we determine a value of r_{skin}^{48} with GHFB+AMP and the constrained GHFB (cGHFB) in which the calculated value is fitted to $r_p(\text{exp})$. For r_{skin}^{48} , the cGHFB result is $r_{\text{skin}}^{48} = 0.19$ fm, while $r_{\text{skin}}^{48} = 0.159$ fm for GHFB+AMP. We should take the upper and the lower bound of GHFB+AMP and cGHFB. Our result is

$$r_{\text{skin}}^{48} = 0.159 - 0.19 \text{ fm.} \quad (9)$$

Our result is consistent with $r_{\text{skin}}^{48}(\text{E1pE})$, $r_{\text{skin}}^{48}(\sigma_I)$, $r_{\text{skin}}^{48}(\text{tPREX})$ and $r_{\text{skin}}^{48}(\text{tE1pE})$, as shown in Fig. 2. The figure also shows that our result is also consistent with the coupled-cluster one of Eq. (8).

We recapitulate our models in Sec. II, and show our results for neighbor nuclei of ^{48}Ca in Sec. III.

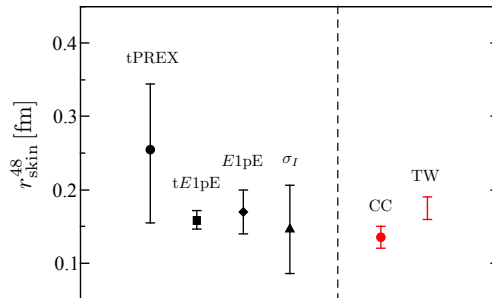


FIG. 2. Comparison among four data and two theoretical results of coupled-cluster theory and this work (TW) for r_{skin}^{48} ; namely, $r_{\text{skin}}^{48}(\text{tPREX})$, $r_{\text{skin}}^{48}(\text{tE1pE})$, $r_{\text{skin}}^{48}(\text{E1pE})$, $r_{\text{skin}}^{48}(\sigma_I)$, $r_{\text{skin}}^{48}(\text{CC})$, $r_{\text{skin}}^{48}(\text{TW})$.

II. MODELS

We recapitulate GHFB, GFHB+AMP and cGHFB.

A. GFHB+AMP

In GHFB+AMP, the total wave function $|\Psi_M^I\rangle$ with the AMP is defined by

$$|\Psi_M^I\rangle = \sum_{K,n=0}^N g_{Kn}^I \hat{P}_{MK}^I |\Phi_n\rangle, \quad (10)$$

where \hat{P}_{MK}^I is the angular-momentum-projector and the $|\Phi_n\rangle$ for $n = 0, 1, \dots, N$ are mean-field (GHFB) states, where $N + 1$ is the number of the states. The coefficients g_{Kn}^I are obtained by solving the Hill-Wheeler equation

$$\sum_{K'n'} \mathcal{H}_{Kn,K'n'}^I g_{K'n'}^I = E_I \sum_{K'n'} \mathcal{N}_{Kn,K'n'}^I g_{K'n'}^I, \quad (11)$$

with the Hamiltonian and norm kernels defined by

$$\left\{ \begin{array}{l} \mathcal{H}_{Kn,K'n'}^I \\ \mathcal{N}_{Kn,K'n'}^I \end{array} \right\} = \langle \Phi_n | \left\{ \begin{array}{l} \hat{H} \\ 1 \end{array} \right\} \hat{P}_{K'K'}^I | \Phi_{n'} \rangle. \quad (12)$$

For even nuclei, there is no blocking state, i.e., $N = 0$ in the Hill-Wheeler equation. We can thus perform GHFB+AMP. However, we have to find the value of β at which the ground-state energy becomes minimum. In this step, the AMP has to be performed for any β , so that the Hill-Wheeler calculation is still heavy. In fact, the AMP is not taken for mean field calculations in many works; see for example Ref. [26]. The reason why we do not take into account γ deformation is that the deformation does not affect σ_R [27]. As for GHFB, meanwhile, we do not have to solve the Hill-Wheeler equation.

For odd nuclei, we must put a quasi-particle in a level. The number N of the blocking states are very large. This makes

it difficult to solve the Hill-Wheeler equation. Furthermore, we have to confirm that the resulting $|\Psi_M^I\rangle$ converges as N goes up for any set of two deformations β and γ . This procedure is extremely time-consuming. For this reason, we do not consider the AMP for odd nuclei. As for GHFB, meanwhile, we do not have to solve the Hill-Wheeler equation, since we consider the one-quasiparticle state with the lowest energy. However, it is not easy to find the values of β and γ at which the energy becomes minimum in the β - γ plane.

As a result of the heavy calculations for even nuclei, we find that β is small for GHFB+AMP; see the table I of Ref. [18] for the values of β . Meanwhile, the mean-field (GHFB) calculations yield that the energy surface becomes minimum at $\beta = 0$. The fact that $\beta = 0$ for GHFB and small for GHFB+AMP yields small difference between GHFB results and GHFB+AMP ones. Therefore, we consider GHFB+AMP for even nuclei and GHFB for odd nuclei.

B. Constrained-GFHB

The difference between $r_p(\text{GHFB} + \text{AMP})$ and $r_p(\text{exp})$ is largest for ^{48}Ca in $^{40-52}\text{Ca}$. In order to fit r_p to the central value of $r_p(\text{exp})$, one use constrained HFB; for example, see Ref. [28]. In the framework of GHFB, we modify the Hamiltonian as

$$\hat{H}_{\text{constraint}} \equiv \hat{H} + \lambda \hat{Q} \quad (13)$$

with

$$\hat{Q} = \hat{r}_p^2 - [r_p(\text{exp})]^2, \quad (14)$$

and take the expectation value $\langle \lambda | \hat{Q} | \lambda \rangle$ of \hat{Q} with the constrained-GHFB (cGHFB) solution $|\lambda\rangle$. The $r_p(\text{cGHFB})$ determined by cGHFB agrees with $r_p(\text{exp})$ under the condition

$$\frac{d\langle \lambda | \hat{Q} | \lambda \rangle}{d\lambda} \Big|_{\lambda=0} = 0. \quad (15)$$

In actual calculations, we use the augmented Lagrangian method [29].

III. RESULTS FOR NEIGHBOR NUCLEI OF ^{48}Ca

As neighbor nuclei of ^{48}Ca , we consider $^{42-51}\text{Ca}$, since the data are available for $r_{\text{skin}}, r_m, r_n, r_p$.

Figure 3 shows $r_p, r_n, r_m, r_{\text{skin}}$ as a function of A . As for r_p , the results of GHFB+AMP and GHFB do not reproduce the data [11] for $^{39-52}\text{Ca}$. For $^{42,44,46,48,50}\text{Ca}$, we then do cGHFB calculations to fit the theoretical value to the central value of $r_p(\text{exp})$.

The cGFHB results hardly change the values of $r_n, r_m, r_{\text{skin}}$ except for r_{skin}^{48} ; see Table I for the numerical values of cGHFB and Table II for the numerical values of GHFB and GHFB+AMP. The deviation for r_p is thus not important except for r_{skin}^{48} . We then take the lower and the upper bound

of GHFB+AMP and cGHFB, as shown in our conclusion in Sec. I.

As for r_{skin} , the results of GHFB, GHFB+AMP, cGHFB reproduce the data [10] for $^{42-48}\text{Ca}$, but underestimate the data for $^{49-51}\text{Ca}$. The difference between GHFB+AMP and GHFB is small for even Ca isotopes, indicating that effects of AMP are small. Eventually, for $^{42,44,46,48}\text{Ca}$, cGHFB reproduce $r_{\text{skin}}(\sigma_I), r_m(\sigma_I), r_n(\sigma_I), r_p(\text{exp})$, while GHFB+AMP does $r_{\text{skin}}(\sigma_I), r_m(\sigma_I), r_n(\sigma_I)$.

The data on r_m has a kink at $A = 48$. Qualitatively, r_m may be in inverse proportion to the binding energy per nucleon, E_B/A . We then consider a dimensionless quantity $\alpha \equiv r_m E_B / (A \hbar c)$, where the central values of data [10, 23] are taken for r_m and E_B/A . The values of α are tabulated in Table III. The average of α and its error are

$$\alpha = 0.1535(9) \quad (16)$$

for $^{42-51}\text{Ca}$, indicating that r_m is in inverse proportion to E_B/A . We can say that the kink comes from the shell effect.

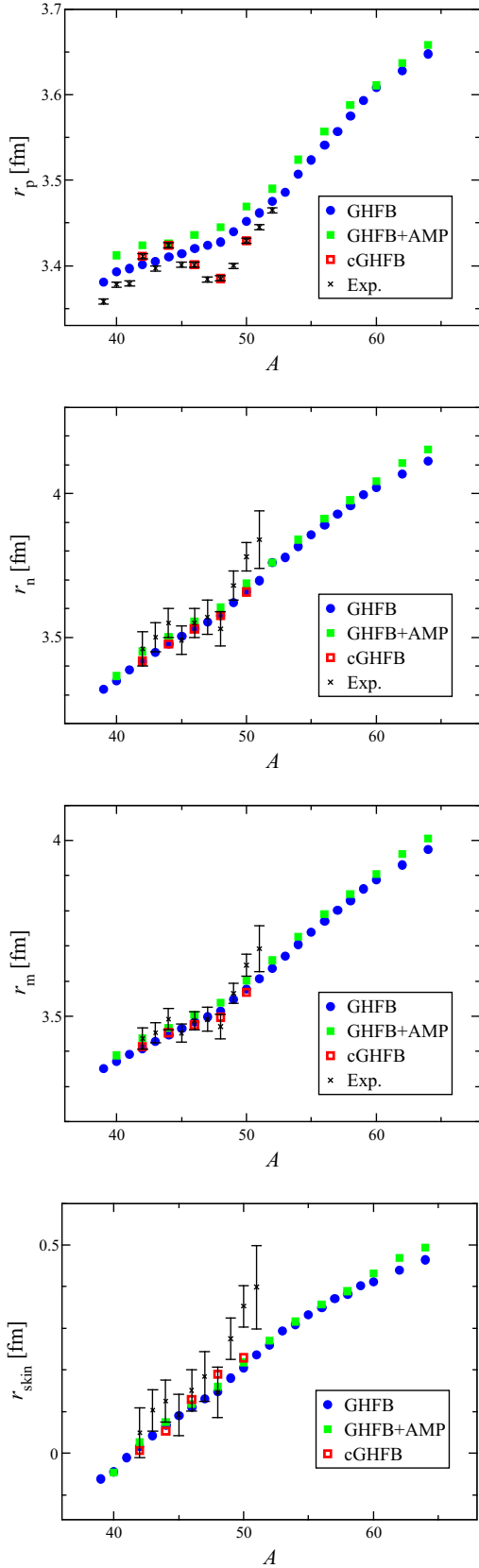


FIG. 3. A dependence of r_p , r_n , r_m , r_{skin} . Closed circles denote the GHFB results, while closed squares correspond to the GHFB+AMP results. Open squares show the results of cGHFB for $^{42,44,46,48,50}\text{Ca}$. Experimental data are taken from Refs. [10, 11].

TABLE I. Radii of constrained GHFB for $^{42,44,46,48,50}\text{Ca}$.

A	r_n fm	r_p fm	r_m fm	r_{skin} fm
42	3.417	3.411	3.414	0.006
44	3.477	3.424	3.453	0.053
46	3.530	3.401	3.475	0.129
48	3.575	3.385	3.497	0.190
50	3.658	3.429	3.568	0.229

TABLE II. Radii for Ca isotopes. The superscript “AMP” stands for the results of GHFB+AMP, and no superscript corresponds to those of GHFB.

A	r_n^{AMP} fm	r_p^{AMP} fm	r_m^{AMP} fm	$r_{\text{skin}}^{\text{AMP}}$ fm	r_n fm	r_p fm	r_m fm	r_{skin} fm
39					3.320	3.381	3.351	-0.061
40	3.366	3.412	3.389	-0.046	3.349	3.393	3.371	-0.044
41					3.387	3.397	3.392	-0.010
42	3.451	3.424	3.438	0.026	3.417	3.401	3.409	-0.010
43					3.448	3.405	3.428	0.043
44	3.501	3.426	3.467	0.075	3.477	3.410	3.447	0.067
45					3.504	3.414	3.465	0.090
46	3.555	3.436	3.504	0.118	3.530	3.420	3.483	0.110
47					3.554	3.424	3.499	0.130
48	3.604	3.445	3.539	0.159	3.576	3.428	3.515	0.148
49					3.621	3.440	3.548	0.181
50	3.687	3.469	3.601	0.218	3.658	3.452	3.577	0.206
51					3.698	3.462	3.607	0.236
52	3.760	3.490	3.659	0.270	3.734	3.475	3.659	0.270
53					3.779	3.486	3.671	0.293
54	3.840	3.524	3.726	0.316	3.817	3.507	3.705	0.310
55					3.856	3.524	3.739	0.332
56	3.913	3.557	3.790	0.357	3.891	3.541	3.770	0.350
57					3.928	3.557	3.802	0.370
58	3.977	3.588	3.847	0.389	3.958	3.575	3.830	0.383
59					3.995	3.593	3.863	0.402
60	4.043	3.611	3.904	0.432	4.020	3.608	3.888	0.412
62	4.106	3.637	3.961	0.469	4.067	3.628	3.931	0.439
64	4.153	3.658	4.005	0.494	4.113	3.648	3.974	0.465

ACKNOWLEDGEMENTS

TABLE III. Numerical values of $r_m(\sigma_I)$ for $^{42-51}\text{Ca}$. The $r_m(\sigma_I)$ are taken from Ref. [10], and the data on E_B/A are from Ref. [23].

A	$r_m(\sigma_I)$ fm	E_B/A MeV	α
42	3.437	8.616563	0.1501
43	3.453	8.600663	0.1505
44	3.492	8.658175	0.1532
45	3.452	8.630545	0.1510
46	3.487	8.66898	0.1532
47	3.491	8.63935	0.1528
48	3.471	8.666686	0.1524
49	3.565	8.594844	0.1553
50	3.645	8.55016	0.1579
51	3.692	8.476913	0.1586

Table IV shows the experimental data [10] on $r_m(\sigma_I)$, $r_n(\sigma_I)$, $r_{\text{skin}}(\sigma_I)$ for $^{42-51}\text{Ca}$, together with $r_p(\text{exp})$ [11].

TABLE IV. Numerical values of $r_p(\text{exp})$, $r_m(\sigma_I)$, $r_n(\sigma_I)$, $r_{\text{skin}}(\sigma_I)$ for $^{42-51}\text{Ca}$. The numerical values on $r_m(\sigma_I)$, $r_n(\sigma_I)$, $r_{\text{skin}}(\sigma_I)$ are taken from Ref. [10], where the systematic error is included. The $r_p(\text{exp})$ are deduced from the electron scattering [11]. Note that Tanaka *et al.* provide us the numerical values of $r_m(\sigma_I)$, $r_{\text{skin}}(\sigma_I)$, $r_n(\sigma_I)$.

A	$r_p(\text{exp})$ fm	$r_m(\sigma_I)$ fm	$r_n(\sigma_I)$ fm	$r_{\text{skin}}(\sigma_I)$ fm
42	3.411 ± 0.003	3.437 ± 0.030	3.46 ± 0.06	0.049 ± 0.06
43	3.397 ± 0.003	3.453 ± 0.029	3.50 ± 0.05	0.103 ± 0.05
44	3.424 ± 0.003	3.492 ± 0.030	3.55 ± 0.05	0.125 ± 0.05
45	3.401 ± 0.003	3.452 ± 0.026	3.49 ± 0.05	0.092 ± 0.05
46	3.401 ± 0.003	3.487 ± 0.026	3.55 ± 0.05	0.151 ± 0.05
47	3.384 ± 0.003	3.491 ± 0.034	3.57 ± 0.06	0.184 ± 0.06
48	3.385 ± 0.003	3.471 ± 0.035	3.53 ± 0.06	0.146 ± 0.06
49	3.400 ± 0.003	3.565 ± 0.028	3.68 ± 0.05	0.275 ± 0.05
50	3.429 ± 0.003	3.645 ± 0.031	3.78 ± 0.05	0.353 ± 0.05
51	3.445 ± 0.003	3.692 ± 0.066	3.84 ± 0.10	0.399 ± 0.10

We thank Dr. Tanaka and Prof. Fukuda for providing the data on radii and interaction cross sections and helpful comments. M. Y. expresses our gratitude to Dr. Y. R. Shimizu for his useful information.

-
- [1] B. A. Brown, Phys. Rev. Lett. **111**, no. 23, 232502 (2013), [arXiv:1308.3664 [nucl-th]].
- [2] X. Roca-Maza, M. Centelles, X. Vinas and M. Warda, Phys. Rev. Lett. **106**, 252501 (2011), [arXiv:1103.1762 [nucl-th]].
- [3] S. Tagami, N. Yasutake, M. Fukuda and M. Yahiro, arXiv:2003.06168 [nucl-th].
- [4] C. J. Horowitz, S. J. Pollock, P. A. Souder and R. Michaels, Phys. Rev. C **63**, 025501 (2001), [nucl-th/9912038].
- [5] R. Michaels *et al.*, Lead Radius Experiment PREX proposal 2005; <http://hallaweb.jlab.org/parity/prex/>.
- [6] S. Abrahamyan *et al.*, Phys. Rev. Lett. **108**, 112502 (2012), [arXiv:1201.2568 [nucl-ex]].
- [7] A. Ong, J. C. Berengut and V. V. Flambaum, Phys. Rev. C **82**, 014320 (2010), [arXiv:1006.5508 [nucl-th]].
- [8] A. Tamii *et al.*, Phys. Rev. Lett. **107**, 062502 (2011), [arXiv:1104.5431 [nucl-ex]].
- [9] J. Birkhan *et al.*, Phys. Rev. Lett. **118**, no. 25, 252501 (2017), [arXiv:1611.07072 [nucl-ex]].
- [10] M. Tanaka *et al.*, Phys. Rev. Lett. **124**, no. 10, 102501 (2020), [arXiv:1911.05262 [nucl-ex]].
- [11] I. Angeli and K. P. Marinova, Atom. Data Nucl. Data Tabl. **99**, 69 (2013).
- [12] G. Hagen *et al.*, Nature Phys. **12**, no. 2, 186 (2015), [arXiv:1509.07169 [nucl-th]].
- [13] G. Hagen, T. Papenbrock, M. Hjorth-Jensen and D. J. Dean, Rept. Prog. Phys. **77**, no. 9, 096302 (2014), [arXiv:1312.7872 [nucl-th]].
- [14] A. Ekstrom *et al.*, Phys. Rev. C **91**, no. 5, 051301 (2015), [arXiv:1502.04682 [nucl-th]].

- [15] R. F. Garcia Ruiz *et al.*, *Nature Phys.* **12**, 594 (2016), [arXiv:1602.07906 [nucl-ex]].
- [16] K. Hebeler, S. K. Bogner, R. J. Furnstahl, A. Nogga and A. Schwenk, *Phys. Rev. C* **83**, 031301 (2011), [arXiv:1012.3381 [nucl-th]].
- [17] R. J. Furnstahl and K. Hebeler, *Rept. Prog. Phys.* **76**, 126301 (2013), [arXiv:1305.3800 [nucl-th]].
- [18] S. Tagami, M. Tanaka, M. Takechi, M. Fukuda and M. Yahiro, *Phys. Rev. C* **101**, no. 1, 014620 (2020), [arXiv:1911.05417 [nucl-th]].
- [19] S. Tagami, Y. R. Shimizu, and J. Dudek, *J. Phys. G* **42** (2015), 015106.
- [20] M. Toyokawa, K. Minomo, M. Kohno and M. Yahiro, *J. Phys. G* **42**, no. 2, 025104 (2015), Erratum: [*J. Phys. G* **44**, no. 7, 079502 (2017)] [arXiv:1404.6895 [nucl-th]].
- [21] M. Toyokawa, M. Yahiro, T. Matsumoto, K. Minomo, K. Ogata and M. Kohno, *Phys. Rev. C* **92**, no. 2, 024618 (2015), Erratum: [*Phys. Rev. C* **96**, no. 5, 059905 (2017)], [arXiv:1507.02807 [nucl-th]].
- [22] M. Toyokawa, M. Yahiro, T. Matsumoto and M. Kohno, *PTEP* **2018**, 023D03 (2018), [arXiv:1712.07033 [nucl-th]]. See <http://www.nt.phys.kyushu-u.ac.jp/english/gmatrix.html> for Kyushu *g*-matrix.
- [23] the National Nuclear Data Center, NuDat 2.7; <https://nucleus.iaea.org/Pages/nu-dat-2.aspx>.
- [24] O. B. Tarasov *et al.*, *Phys. Rev. Lett.* **121**, 022501 (2018).
- [25] S. Michimasa *et al.*, *Phys. Rev. Lett.* **121**, 022506 (2018).
- [26] S. Hilaire and M. Girod, Hartree-Fock-Bogoliubov results based on the Gogny force; <http://www-phynu.cea.fr/science-en-ligne/carte-potentiels-microscopiques/carte-potentiel-nucleaire-eng.htm>.
- [27] T. Sumi, K. Minomo, S. Tagami, M. Kimura, T. Matsumoto, K. Ogata, Y. R. Shimizu and M. Yahiro, *Phys. Rev. C* **85**, 064613 (2012), [arXiv:1201.2497 [nucl-th]].
- [28] E. Khan, J. Margueron, G. Colo, K. Hagino and H. Sagawa, *Phys. Rev. C* **82**, 024322 (2010) doi:10.1103/PhysRevC.82.024322 [arXiv:1005.1741 [nucl-th]].
- [29] A. Staszczak, M. Stoitsov, A. Baran and W. Nazarewicz, *Eur. Phys. J. A* **46**, 85 (2010), [arXiv:1006.4137 [nucl-th]].